

Article

# Thermal Conductivity of Suspension of Aggregating Nanometric Rods

Amine Ammar <sup>1,2,\*</sup>, Francisco Chinesta <sup>3</sup> and Rodolphe Heyd <sup>4</sup>

<sup>1</sup> LAMPA, ENSAM Angers, 2 Boulevard du Ronceray, BP 93525, 49035 Angers Cedex 01, France

<sup>2</sup> UMSSDT, ENSIT Université de Tunis, 5 Avenue Taha Hussien Montfleury, 1008 Tunis, Tunisia

<sup>3</sup> High Performance Computing Institute (ICI), Ecole Centrale de Nantes, 1 rue de la Noe, 44300 Nantes, France; francisco.chinesta@ec-nantes.fr

<sup>4</sup> ICMN, UMR7374, CNRS-University of Orléans, 1b rue de la Férellerie, 45100 Orléans, France; rodolphe.heyd@univ-orleans.fr

\* Correspondence: amine.ammar@ensam.eu; Tel.: +33-2-4120-7323

Academic Editors: Kevin H. Knuth and Adom Giffin

Received: 10 November 2016; Accepted: 24 December 2016; Published: 31 December 2016

**Abstract:** Enhancing thermal conductivity of simple fluids is of major interest in numerous applicative systems. One possibility of enhancing thermal properties consists of dispersing small conductive particles inside. However, in general, aggregation effects occur and then one must address systems composed of dispersed clusters composed of particles as well as the ones related to percolated networks. This paper analyzes the conductivity enhancement of different microstructures scaling from clusters dispersed into a simple matrix to the ones related to percolated networks exhibiting a fractal morphology.

**Keywords:** nanofluids; thermal homogenization; aggregation kinetics; percolation

**PACS:** 05.20.Dd; 05.10.Ln; 05.10.Gg

## 1. Introduction

It is crucial today to explore techniques of energetic and thermal performances enhancement in many fields of science to save on many energy resources. Many simple liquids (water, ethylene glycol, oils) are usually used as heat transfer fluids: in thermal engines (coolants, lubricating oils, etc.), in solar panels of individual water heaters, in the collectors of industrial solar power plants, in power transformers (industry, power distribution network), and in industrial installations (cutting oils, coolants). Unfortunately, these usual liquids all have low thermal conductivities at ambient or industrial temperature. We can find, for example, in [1], some values of usual thermal conductivity of fluids: water, 0.58 W/(m·K); ethylene glycol, 0.18 W/(m·K), which are very low compared to usual metals such as: iron, 80 W/(m·K); copper, 400 W/(m·K); silver, 430 W/(m·K); graphite, 1000 to 1500 W/(m·K); carbon nanotubes, 2000 to 2500 W/(m·K); suspended graphene, 2500 W/(m·K) and diamond, 2500 W/(m·K). Any increase in the thermal conductivity promotes the exchanges of thermal energy and consequently the extraction ability of the heat from fluids.

The use of fluids containing metallic or semi-conductive particles in homogeneous and stable suspensions is one of the solutions studied for several years for the improvement of thermal transfer. Suspensions of microscopically sized conductive particles are contemplated and used for many years. However, due to the size of the suspended particles, they present problems that limit their industrial applications: abrasion and high risk of sedimentation and clogging. Moreover, the surface-to-volume ratio, which plays a predominant role in all conductive transport phenomena, can be significantly improved with particles of smaller sizes.

With the constant progress of nanotechnologies and the synthesis of specific nanoparticles, the idea of using thermal nanofluids has attracted a lot of interest in the scientific community [2], but also in industry. The scientific literature on the subject is vast and diverse. It covers both the fundamental (theoretical) aspects of the static thermal modeling, rheological properties of nanofluids and their synthesis, numerical modeling as well as the thermal and rheological characterization of suspensions in the laboratory.

In [3], a theoretical model is proposed to describe heat transfer performance of the nanofluids. Others works such as [4] are based on molecular dynamic simulations and aim to explain the differences in thermal conductivity between nanofluids based on metal (Cu) and metal oxide (CuO) nanoparticles. A large part of published works related to the thermal conductivities of nanoparticles suspensions have been based on experimental measurement. In [5], effective thermal conductivity measurements of alumina/water and copper oxide/water nanofluids are performed and the effects of particle volume fraction, temperature and particle size were investigated. High aspect ratio fillers (carbon nanotubes (CNTs), silver nanowires, copper nanowires) are considered in [6]. It is found there that silver nanofluid has the highest thermal conductivity compared with copper and CNT nanofluids. In [7], authors analyze several mechanisms affecting the thermal conductivity of Alumina based nanofluid, such as layering, Brownian motion, clustering, ballistic phonon motion, thermal boundary resistance and mass difference scattering. In [8], authors look for the specific case when the base fluid is a mixture of ethylene glycol and water. Thermal conductivity has been estimated experimentally at different volume concentrations and temperatures. Other works are related to the coupling with kinematics and rheological response. The effect of viscosity is studied in [9]. The kinematic effects are also studied in [10], where an experimental method of studying the heat transfer behavior of buoyancy-driven nanofluids was addressed. These studies open opportunities for many application fields. For example, an interesting applications, related to wind turbines and solar collectors, is found, respectively, in [11,12]. The reader can find in [13] and in the references therein an overview of experimental results about the heat transfer capabilities of nanofluids, which is presented using widely scattered available information from diverse literature sources.

The main aim of the present work is the analysis of thermal properties, in particular the equivalent thermal conductivity, of suspensions involving manometric rods suspended in a Newtonian (purely viscous) fluid. When using particles highly conductive in a poorly conducting matrix, even at very low particle concentration (less than 1 vol.%), it has been observed that the resultant equivalent fluid (suspension) increases (sometimes more than 100%) its apparent thermal conductivity significantly.

In literature, many phenomena are found to be responsible for thermal conductivity enhancement: Brownian motion, ordered liquid layer formation at the nanoparticle surface, interfacial thermal resistance, fractal structuring, cluster formation, thermal conductivity of particles, viscosity of the host fluid, sonication, and surface treatment of the nanoparticles, among many others. In the vast literature about the thermal properties of nanofluids, we can also find a large dispersion of the experimental results. For example, in [14], it is mentioned, in regard to the effect of the particle volume fraction for example, that enhancements within and beyond the effective medium theory (random dispersion of the nanoparticles through the host fluid) are reported in the literature. The effects of the nanoparticle sizes and nanofluid temperature have also been analyzed in this review; they also show a vast dispersion in the enhancements of the thermal conductivity of nanofluids.

The reasons for these contradictory reports are certainly multiple. We can mention, for example: the choices of the nanoparticle surface chemical treatments; the choice of the host fluid and of the method of the nanoparticle dispersion; and, even sometimes, the choice of the measurement technique.

Taking into account all of these aspects, we have chosen to adopt the following point of view, which consists of analyzing the sole influence of the organization of the nanoparticles within the nanofluid, on its thermal conductivity. The Brownian motion must be viewed in this study as a way to construct two realistic types of structured patterns: fractal skeletons (as observed experimentally and

mentioned in [15]) and micrometric aggregates (as also observed experimentally), and not as a way to promote heat transfer at the microscopic scale.

Thus, we try in this work to answer the following fundamental question: to what extent is the organization of the nanoparticles inside nanofluids essential for improving the thermal conductivity of nanofluids?

This question is fundamental in many aspects. We will prove that the effect of organization is crucial in the enhancement. In addition, the percolation or not of the particles is determinant for final conductivity. This is demonstrated by calculating the heat transfer homogenization based on Fourier's law without taking into account the Brownian induced conductivity.

In most existing works, the values of the volume fraction considered was much lower than the values used in the present paper. As it has been previously indicated, the present work aims to show the effect of the structure on the thermal conductivity enhancement. In many experiments concerning low viscosity liquids, the Brownian induced conductivity is at the origin of the enhancement of thermal performances at low concentration. In this case, the simulations have to be done with another approach based on the Green–Kubo method, which is used to obtain the thermal conductivity of the nanofluid from the heat autocorrelation function (see for example [16,17]). Our strategy in the present work is different. We address heat transfer from the homogenized thermal conductivity related to conduction (Fourier's law). Such an approach does not take into account Brownian motion for calculating the effective conductivity. Brownian motion has only been used here for developing microstructures (random fractals or clusters) as experimentally observed in many situations where nanoparticles agglomerate inside the host fluid. Moreover, the approach here proposed could be useful to explain thermal conductivity enhancements for some fluids where the viscosity effects are preponderant. In fact, in [3,18], we observe almost the same enhancement at a low concentration. Even if it is shown in [19] that high enhancements of the thermal conductivity can be found for low concentrations, compared to our simulations, it is not in contradiction with our study because we only focused here on structuration effects and not on the other different factors previously mentioned that could promote an extra-thermal conductivity enhancement.

It is well known that particles, suspended into a viscous medium, tend to create aggregates that could reach larger space scales, and, in some cases, they are resolvable at the eyes scale. The modeling of such aggregates requires the consideration of kinetic models at the meso-scale accounting for the flow induced aggregation/disaggregation mechanisms [20]. As soon as these particles are functionalized in order to avoid aggregation mechanisms, no aggregates are observed at the resolvable scales, and standard models developed for addressing dilute suspensions work well for describing their main rheological features [21].

In many cases when addressing materials or meta-materials (functionalized materials exhibiting gradients of properties originated by different concentrations and orientations of the dispersed charges) forming processes, after dispersing the particles, a microstructure develops inside and can be frozen by transforming the fluid phase into a solid (e.g., by polymerizing a thermoset resin).

The final properties of the resulting microstructured fluid or solid become radically different from a simple mixing rule as soon as percolation occurs. In these cases, an appropriate homogenization strategy is compulsory for evaluating the final properties. There are numerous works addressing homogenization strategies for systems consisting of perfectly dispersed particles into a matrix (i.e., in the absence of aggregates). In [22], a reinforced polymer consisting of a population of  $\mathcal{N}$  nanometric conducting rods immersed into an insulating polymer matrix was assumed. At the microscopic scale, the system can be described from the specification of the position of the centre of gravity  $\mathcal{G}_i$  and orientation  $\mathbf{p}_i$  of each rod in the population, with  $i = 1, \dots, \mathcal{N}$ .

The microscopic description, despite the fact of being the finest one, is too heavy from both the computational and the experimental points of view. For this reason, coarser descriptions are preferred. At the mesoscopic scale, the rods' individuality is substituted with an orientation distribution function  $\Psi(\mathbf{x}, \mathbf{p})$  given the fraction of rods that at position  $\mathbf{x}$  align along direction  $\mathbf{p}$ . Because this probability

distribution function—pdf—is defined in a space of high dimensionality (involving the physical space  $\mathbf{x}$  and the conformation coordinates  $\mathbf{p}$ ), the solution of its associated balance equation (the so-called Fokker–Planck equation) remains cumbersome, even if advanced numerical discretization techniques have been proposed for alleviating or circumventing the curse of dimensionality that high dimensionality entails [23,24].

Finally, macroscopic descriptions constitute the coarsest level of description but the one leading to faster simulations. This description is based on the use of the probability distribution function moments, also known as orientation tensors, being the expression of the second moment given by

$$\mathbf{a}(\mathbf{x}) = \oint \mathbf{p} \otimes \mathbf{p} \Psi(\mathbf{x}, \mathbf{p}) \, d\mathbf{p}. \quad (1)$$

In order to quantify the rod network, we introduced in [22] the density of rod contacts  $\mathcal{C}(\mathbf{x}, \mathbf{p})$  for a rod with orientation  $\mathbf{p}$ , depending on the two main microstructure descriptors: (i) the rods concentration  $\phi(\mathbf{x})$ ; and (ii) the orientation distribution  $\Psi(\mathbf{x}, \mathbf{p})$ . Its evaluation follows the simple geometrical construction depicted in Figure 1 in which first approximation rods are assumed rigid and straight. Similar descriptors were proposed in [25–28].

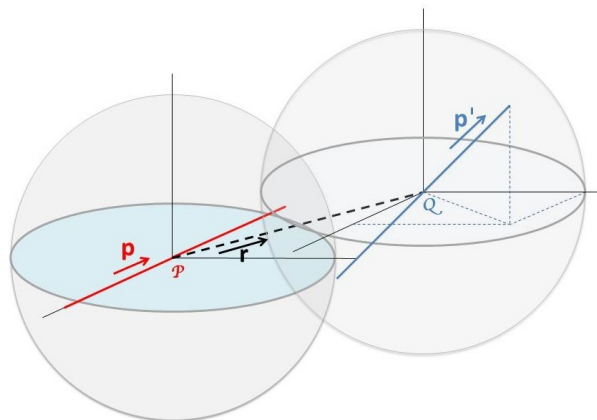


**Figure 1.** Evaluating rod contacts.

It can be expected that the conductivity at position  $\mathbf{x}$  along direction  $\mathbf{p}$  scales with the number of contacts  $\phi(\mathbf{x})\mathcal{C}(\mathbf{x}, \mathbf{p})\Psi(\mathbf{x}, \mathbf{p})$ . Thus, the conductivity becomes local and directional. One can expect that percolation along direction  $\mathbf{p}$  occurs locally (at position  $\mathbf{x}$ ) when the number of contacts is higher than a threshold value  $\mathcal{T}$ . Lower values imply an infinite local directional resistivity. Thus, percolation could be considered local and directional, allowing us to create a network in which to evaluate the effective conductivity.

When considering electrical properties, the calculation at the network level was carried out by using usual Kirchhoff's laws [22]. The question arising immediately concerns the existence of an appropriate fully-macroscopic description modeling thermal conductivity in a perfectly dispersed suspension composed of rods. This modeling framework, with some simplifying assumptions, is described in Section 2. Then, we will focus on more complex scenarios, the ones involving aggregation mechanics leading to the creation of macroscopic clusters (dispersed into the suspending matrix) and percolated networks, both addressed in Section 3. The computational thermal homogenization of such complex microstructures is addressed in Section 4 before then discussing some numerical results in Section 5.

Different assumptions are considered in the sequel: (i) advective heat fluxes are neglected when the matrix becomes solid in the final part in which the thermal properties are evaluated; (ii) the suspending fluid is assumed viscous and at rest, making possible the particle movement, but remaining insensible to thermal dependencies of its density when addressing thermal homogenization, the viscous forces

being preponderant with respect to buoyancy, in all the cases considered here; and (iii) the thermal conductivity contrast between the matrix and the particles is assumed to be large.

## 2. On the Macroscopic Thermal Conductivity of Perfectly Dispersed Rod Suspensions

When the suspension involves perfectly dispersed rods, a homogenized thermal conductivity can be derived almost analytically. This model only involves the orientation distribution second moment, also called the “orientation tensor” introduced above. In the case of more complex particle shapes, computational homogenization (described in Section 4) represents a valuable alternative for evaluating the equivalent conductivity. When individual particles of any shape aggregate to create more complex microstructures, computational homogenization seems compulsory for calculating homogenized properties as discussed later.

Before addressing more complex scenarios, we start our analysis by describing the homogenization procedure in the case of a perfectly dispersed suspensions of rods, assuming no thermal interfacial resistance between the rods and the matrix as previously indicated, while ignoring advective heat transfer.

The matrix thermal conductivity is assumed, for the sake of simplicity and without loss of generality, isotropic, and expressed by the scalar  $k_m$ , whereas the bulk isotropic conductivity of the rod particles is expressed by  $k_p$ , with, as indicated above,  $k_p \gg k_m$ . The thermal contrast  $c$  is defined from  $c = k_p/k_m$ , with, in our case,  $c \gg 1$ . The heat flux  $\mathbf{Q}_m$  through the host matrix is calculated according to the standard Fourier law

$$\mathbf{Q}_m \approx -(1 - \phi)k_m \nabla T, \quad (2)$$

where  $\nabla T$  is the given macroscopic gradient of temperature, supposed to be constant within the representative volume element—RVE— $\omega$ .

Now, in a given rod with orientation  $\mathbf{p}$ , the heat flux is assumed directed in the rod direction (we are assuming high thermal contrast), and, consequently, the effective temperature gradient along the rod is written as

$$(\nabla T \cdot \mathbf{p})\mathbf{p} = (\mathbf{p} \otimes \mathbf{p}) \cdot \nabla T, \quad (3)$$

and, consequently, the heat flow inside the rod reads

$$\mathbf{q}_p(\mathbf{p}) \approx -k_p(\mathbf{p} \otimes \mathbf{p}) \cdot \nabla T. \quad (4)$$

By adding the contribution of all the rods in  $\omega$ , it results

$$\mathbf{Q}_p = \int_S \mathbf{q}_p(\mathbf{p})\phi\Psi(\mathbf{p})d\mathbf{p} \approx -k_p\phi \mathbf{a} \cdot \nabla T. \quad (5)$$

Now, with the total heat flux being  $\mathbf{Q} = \mathbf{Q}_m + \mathbf{Q}_p$ , we obtain

$$\mathbf{Q} = -(k_m(1 - \phi)\mathbf{I} + k_p\phi \mathbf{a}) \cdot \nabla T = -k_m((1 - \phi)\mathbf{I} + c\phi\mathbf{a}) \cdot \nabla T, \quad (6)$$

with  $\mathbf{I}$  the identity tensor. Thus, we can define the homogenized thermal conductivity tensor  $\mathbf{K}$  as

$$\mathbf{K} = -k_m((1 - \phi)\mathbf{I} + c\phi\mathbf{a}). \quad (7)$$

## 3. Generating Microstructures and Networks

In this section, we consider different ways of creating more complex microstructures from individual particles when clustering mechanisms act. In particular, we are considering two different algorithms: (i) the DLAA (Diffusion Limited Aggregation algorithm) and (ii) the MDAa (Molecular Dynamics Aggregation algorithm)—both operating at different levels of concentration.

In all the cases studied in this paper, we performed different runs of simulation, in order to extract the average and variability of the computed results.

### 3.1. From DLA to Enhanced-DLA

First, we start with a fully empty space and put one particle somewhere. Now, a second particle is randomly introduced and it keeps moving randomly until it reaches the first one. Then, both are attached and assumed at rest while a third particle is introduced and randomly moves until reaching the cluster composed by the previously attached particles. The procedure repeats until all particles have been introduced and been attached to the particle network.

The main issues of such a strategy are that it does not address conveniently the fact that the systems proceed from a given constant particle concentration and the fact of addressing Brownian motion more consistently. To better address both questions, we propose considering a lattice model that contains all possible particle locations and defines consequently the discrete particle jumps during their motion. The process parameters are: (i) the particle concentration  $C$ , the diffusion  $D$  quantifying the Brownian motion and the characteristic length  $L$  of the representative volume element—RVE—with respect to the particle equivalent diameter. Thus, for example,  $L = 10$  means that the RVE size is ten times the particle diameter. For non-spherical particles, an equivalent diameter can be defined from excluded volume considerations.

Thus, the enhanced-DLA proceeds by putting all the particles into the simulation box (RVE), a number that is determined from the concentration. One of the simulated particles is located at the center of the computational box and it is kept at rest all throughout the simulation. The remaining particles, all except the one attached at the centre of the RVE, move randomly. Periodic boundary conditions are assumed on the RVE boundaries, implying that one particle leaving the box from one of its faces, comes in from the opposite face. As soon as a moving particle collides with the one kept at rest at the box center, it is glued to the first and occupies the neighbor lattice position (associated with the arrival direction). Then, both (the initial one and the just glued) are kept at rest while waiting for the arrival of the third particle, and so on. Thus, the particle network continues growing until all particles join it.

The enhanced DLA algorithm is illustrated in Figure 2 for  $D = 5$ . In this figure, black particles are those belonging to the network assumed at rest. Around three moving particles (numbered white circles) are depicted, and, at the present time, all of them move  $D$  lattice units ( $D = 5$  in this case), making directional random choices at each of the  $D - 1$  lattice jumps (we do not consider the possibility of coming back during a lattice jump). In what follows, unit jumps on the lattice will be denoted by N (north), S (south), E (east) or W (west). In the random particle movement, some constraints apply:

- The random path of a particle does not cross any other free (moving) particles.
- If a random path ends at a gluing point, the last being a neighbor of the already attached particles (black circles), symbolized by a cross in Figure 2, then the particle is attached to the growing network and kept at rest in the sequel (particle 2 in Figure 2). As soon as the particle joins the network, the set of gluing points is updated by including the neighbors of the just glued particle on the lattice.
- If the random path crosses a gluing point, it is attached to the network, even if it does not complete its  $D - 1$  unit jumps (see particle 1 in Figure 2).
- If the random path ends far enough from the growing network, it remains free and then ready to randomly move at the next time step (particle 3 in Figure 2).

The simulation finishes when all particles have been attached to the network.

Figures 3 and 4 present the resulting microstructures consisting of a single network composed of all the particles, when considering different values of the simulation parameters  $D$  and  $C$ . It can be noticed that the modification of the diffusion parameter  $D$  (from  $D = 1$  to  $D = 16$ ) does not affect the nature of the resulting fractal structure (the fractal dimension remains unchanged); however, its

increase results in a faster development of the particle network. On the other side, by modifying the concentration, the fractal structure is significantly affected. Thus, for discussing the steady-state properties, in what follows, only the concentration will be considered.

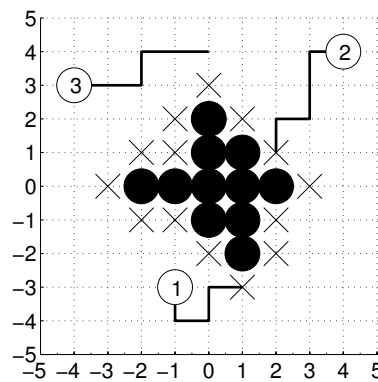


**Figure 2.** Illustrating the DLA algorithm. Each particle moves  $D = 5$  lattice units (horizontal and vertical coordinates refer to lattice units), in random directions, except if, before completing the  $D$  jumps, it reaches the aggregate (particle 1).

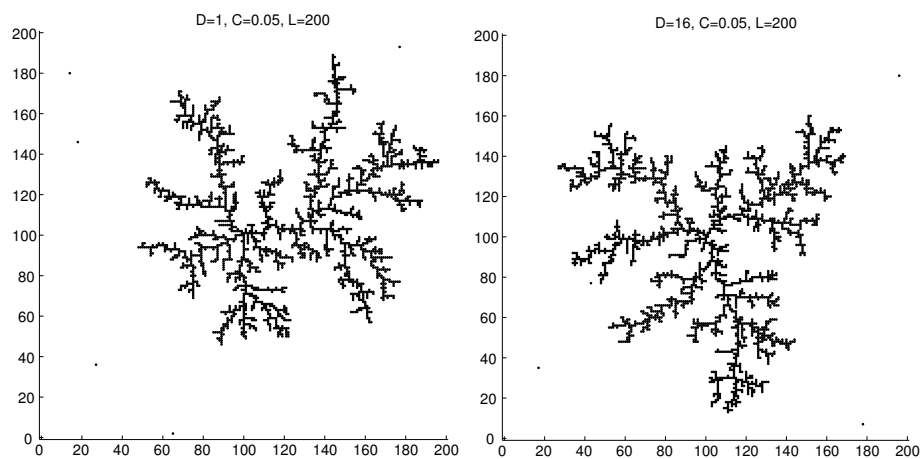


**Figure 3.** DLA-simulated microstructures when varying parameter  $D$  for  $C = 0.05$ .

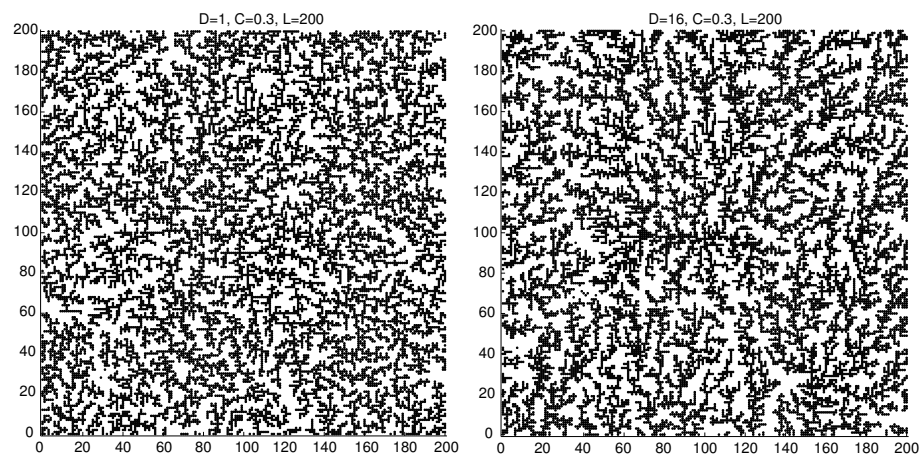


**Figure 4.** DLA-simulated microstructures when varying parameters  $D$  for  $C = 0.3$ .

### 3.2. Molecular Dynamic Aggregation Algorithm

When considering the so-called molecular dynamics aggregation algorithm—MDAa—particles are randomly placed into the RVE and a two-particle interaction potential (the Lennard–Jones potential in the simulations carried out later) is considered acting between each pair of particles  $i$  and  $j$ , according to

$$V(d) = 4\epsilon \left( \left( \frac{\sigma}{d} \right)^{12} - \left( \frac{\sigma}{d} \right)^6 \right), \quad (8)$$

where  $d$  is the distance between the centers of two particles involved in the interaction, and  $\sigma$  and  $\epsilon$  are two model parameters.

Based on this potential, the interaction force acting on the  $i$ -particle induced by the one located at position  $\mathbf{x}_j$  reads

$$\mathbf{F}_{j \rightarrow i} = -\nabla V|_{d(i,j)} \mathbf{n}_{j \rightarrow i}, \quad (9)$$

where  $d(i, j)$  is the mutual distance and  $\mathbf{n}_{j \rightarrow i}$  the unit vector that points from  $\mathbf{x}_j$  to  $\mathbf{x}_i$ .

Thus, the resulting force acting on particle  $\mathbf{x}_i$  is written as

$$\mathbf{F}_i = \sum_{j \neq i} \mathbf{F}_{j \rightarrow i}. \quad (10)$$

The algorithm consists of updating particle velocity and position by using the dimensionless Newton's equation of dynamics, which allows for computing the particle acceleration

$$\mathbf{F}_i(t) = m_i \left. \frac{d^2 \mathbf{x}_i}{dt^2} \right|_t = m_i \mathbf{a}_i(t), \quad (11)$$

and then velocity and position from an adequate (symplectic) integration strategy, as the one of Verlet that reads

$$\mathbf{x}_i(t + \Delta t) = \mathbf{x}_i(t) + \mathbf{v}_i(t)\Delta t + \frac{1}{2} \mathbf{a}_i(t)\Delta t^2, \quad (12)$$

$$\mathbf{v}_i(t + \Delta t) = \mathbf{v}_i(t) + \frac{1}{2} (\mathbf{a}_i(t) + \mathbf{a}_i(t + \Delta t)) \Delta t. \quad (13)$$

When using the MDAa, after introducing randomly all the particles into the RVE, interaction potential applies and particles start moving, creating different clusters within the RVE, with positions and size evolving in time, instead of the single particle network created from DLA-based strategies.

## 4. Calculating the Equivalent Thermal Conductivity

Due to the microscopic heterogeneity (where matrix and particles coexist, the last cluster making part of a single network depending on the microstructure constructor chosen, MDAa or DLAA, respectively, the macroscopic thermal modeling needs a homogenized thermal conductivity that depends on the microscopic details.

We can define the macroscopic temperature gradient  $\nabla T$  at the RVE level from

$$\nabla T = \langle \mathbf{g}(\mathbf{x}) \rangle = \frac{1}{|\omega|} \int_{\omega} \mathbf{g}(\mathbf{x}) \, d\mathbf{x}, \quad (14)$$

where  $\mathbf{g}(\mathbf{x})$  denotes the microscopic temperature gradient.

We also assume the existence of a localization tensor relating the macroscopic temperature gradient (average of its microscopic counterpart)  $\nabla T$  with the microscopic local temperature gradient  $\mathbf{g}(\mathbf{x})$ ,  $\mathbf{L}(\mathbf{x})$ , such that

$$\mathbf{g}(\mathbf{x}) = \mathbf{L}(\mathbf{x}) \cdot \nabla T. \quad (15)$$

Now, we consider the microscopic heat flux  $\mathbf{q}(\mathbf{x})$  at  $\mathbf{x} \in \omega$  according to Fourier's law

$$\mathbf{q}(\mathbf{x}) = -\mathbf{k}(\mathbf{x}) \cdot \mathbf{g}(\mathbf{x}), \quad (16)$$

and its macroscopic counterpart  $\mathbf{Q}$  that is written

$$\mathbf{Q} = \langle \mathbf{q}(\mathbf{x}) \rangle = -\langle \mathbf{k}(\mathbf{x}) \cdot \mathbf{g}(\mathbf{x}) \rangle = -\langle \mathbf{k}(\mathbf{x}) \cdot \mathbf{L}(\mathbf{x}) \rangle \cdot \nabla T, \quad (17)$$

from which the homogenized thermal conductivity can be defined at the RVE level from

$$\mathbf{K} = \langle \mathbf{k}(\mathbf{x}) \cdot \mathbf{L}(\mathbf{x}) \rangle. \quad (18)$$

As  $\mathbf{k}(\mathbf{x})$  is perfectly known everywhere in the representative volume element  $\omega$ , the definition of the homogenized thermal conductivity tensor only requires the computation of the localization tensor  $\mathbf{L}(\mathbf{x})$ . Several approaches are proposed in the literature to define this tensor, according to the choice of the boundary conditions. Our objective here is not to discuss such a choice. For the sake of simplicity, we use essential boundary conditions on  $\partial\omega$  corresponding to the assumption of a uniform temperature gradient on the RVE  $\omega$ . We consider the general 2D case that involves the solution of the two boundary value problems related to the steady state heat transfer model in the microscopic domain  $\omega$  for two different boundary conditions on  $\partial\omega$ :

$$\begin{cases} \nabla \cdot (\mathbf{k}(\mathbf{x}) \cdot \nabla \Theta^1(\mathbf{x})) = 0 \\ \Theta^1(\mathbf{x} \in \partial\omega) = x \end{cases}, \quad (19)$$

and

$$\begin{cases} \nabla \cdot (\mathbf{k}(\mathbf{x}) \cdot \nabla \Theta^2(\mathbf{x})) = 0 \\ \Theta^2(\mathbf{x} \in \partial\omega) = y \end{cases}. \quad (20)$$

It is easy to prove that both solutions verify

$$\begin{cases} \langle \nabla \Theta^1(\mathbf{x}) \rangle = (1, 0)^T \\ \langle \nabla \Theta^2(\mathbf{x}) \rangle = (0, 1)^T \end{cases}, \quad (21)$$

where  $(\cdot)^T$  denotes the transpose. Thus, the localization tensor finally results as

$$\mathbf{L}(\mathbf{x}) = \begin{pmatrix} \nabla \Theta^1(\mathbf{x}) & \nabla \Theta^2(\mathbf{x}) \end{pmatrix}. \quad (22)$$

From a computational point of view, the main difficulty concerns the solution of the two boundary value problems using very fine meshes required to represent accurately all of the microscopic details. In the extreme case of meshes that are too fine, advanced solvers based on the use of separated representations (at the heart of the Proper Generalized Decomposition (PGD)) could be a valuable alternative [29,30].

To check the proposed strategy just described, we consider the DLA-based microstructure depicted in Figure 5. Figure 6 shows both temperature fields  $\Theta^1(\mathbf{x})$  and  $\Theta^2(\mathbf{x})$ .

For the solutions carried out in this study, the mesh size was chosen in order to ensure the numerical convergence, i.e., the mesh-size independence of the computed solutions. Figures 7 and 8 analyze the solution dependence as a function of the number of nodes along the particle diameter, for one and many particles, respectively. It can be seen that when considering ten nodes along the particles' characteristic length, the conductivity becomes almost constant.

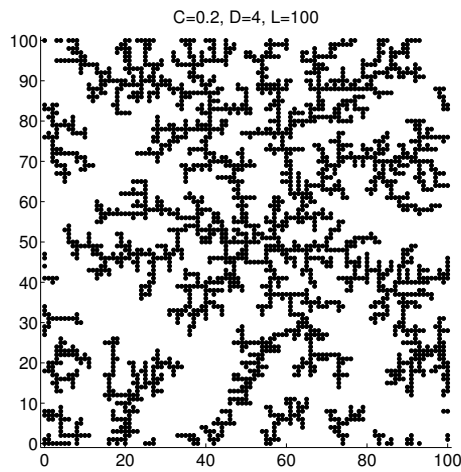


Figure 5. DLA-based microstructure (again horizontal and vertical coordinates refer to lattice units).

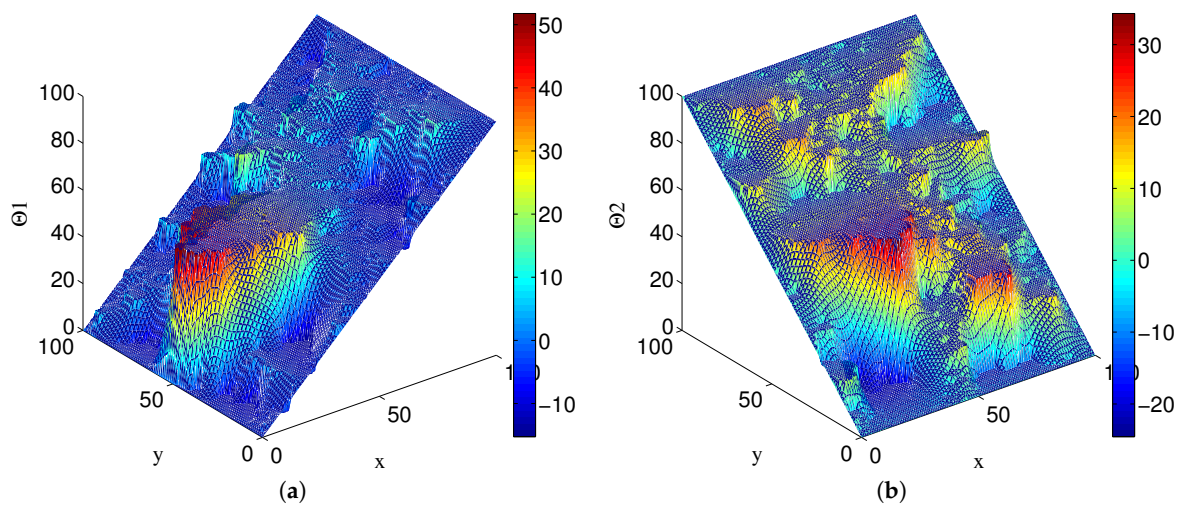


Figure 6. Local temperature fields related to the microstructure depicted in Figure 5. (a)  $\Theta^1(x)$ ; (b)  $\Theta^2(x)$ .

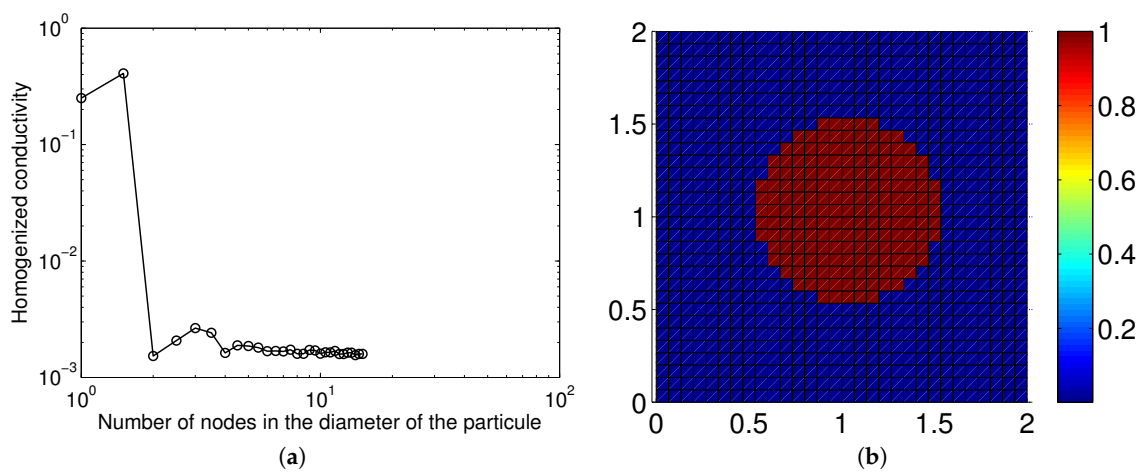
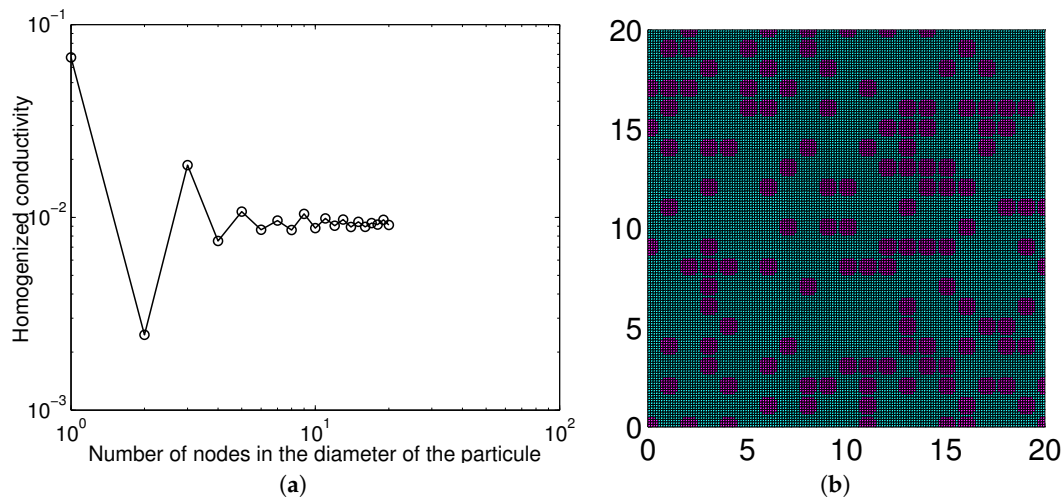


Figure 7. Convergence analysis in a volume containing a single particle. (a) Convergence curve; (b) Microstructure.



**Figure 8.** Convergence analysis when considering many particles. (a) Convergence curve; (b) Microstructure.

## 5. Numerical Results

In order to compare the homogenized thermal conductivity for different microstructures obtained by using the enhanced DLA and MDA algorithms, we proceed from the same initial particle distribution and different values of the associated concentration. The mesh considered ensured the numerical convergence of all of the thermal analyses carried out in the present study.

The value of concentrations used in the field of nanofluids is usually lower than the maximum range that we have considered in our study. It is generally on the order of 0.1% or to 2%. However, as mentioned previously, the dispersion of the experimental results is such that, in many cases reported in the literature, low volume concentrations of nanoparticles do not always lead to spectacular enhancements of the thermal conductivity. In some specific studies, the volume fraction can reach even values up to 9% [5,15]. In the present study, our aim is to focus mainly on the structure-based enhancement effects. For lower concentrations, other numerical strategies are more convenient (the Green–Kubo method and heat autocorrelation function), but, as just indicated, this is not our purpose. In order to compare with some papers in literature, Figure 9 presents an extension of our study results to a volume fraction lower than 2%.

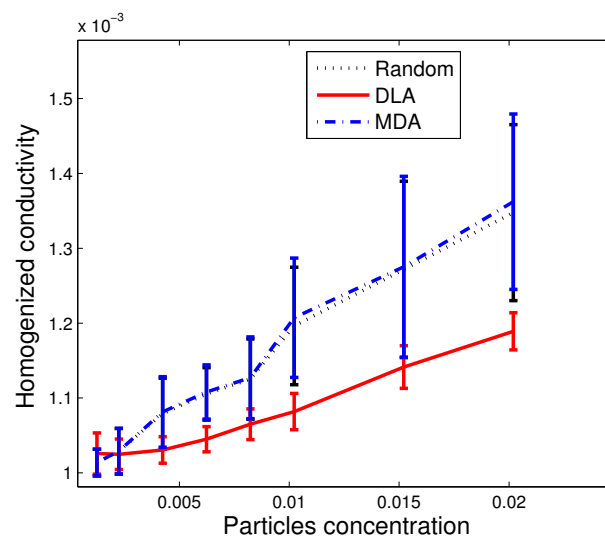


**Figure 9.** Evolution of equivalent conductivity with the particle concentration for low concentrations.

The reported values show the increase of relative conductivity  $k_{suspension}/k_{particle}$  from 0.001 when there are no particles to 0.014 at 2% of volume fraction. These orders of magnitude are the same that are found in some existing works (e.g., [3,18]). Regarding this figure, modification of conductivity is almost the same for random distribution or MD simulation (they almost give the same values of conductivity because low concentration does not promote percolation). However, results of DLA are not significant here as they are related to a small aggregated structure in the middle of the simulation domain.

Figure 10 reports the results found for higher concentrations. It can be seen that, as expected for both kinds of microstructures (the one generated by the enhanced-DLAa and the MDa), the equivalent (homogenized) conductivity increases with the particle concentration. Moreover, the thermal conductivity of the resulting microstructures is larger than the one related to the initial random distribution of particles, all of them being quite similar at very low concentrations. When the concentration increases, the percolated network development seems the most favorable for heat conduction. These numerical results are very similar to the experimental results reported in [15] on the basis of measurements of the thermal conductivity of magnetically polarizable nanofluids. As can be seen in Figure 10, at very large concentrations, our computations show that the MD aggregated microstructures are more favorable to heat conduction than the DL ones. This is a quite interesting result, in the sense that the agglomeration of nanoparticles in the form of individual clusters is not an obstacle to the heat conduction through the colloidal suspensions, as long as the sedimentation can be neglected. This facility can be easily understood by comparing the analyzed microstructure morphology depicted in Figures 11–13, where the superiority of the percolated MD networks can be easily pointed out.

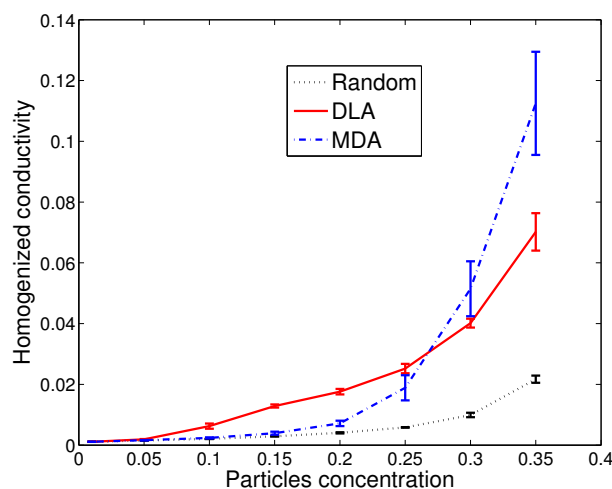


**Figure 10.** Evolution of equivalent conductivity with the particle concentration at higher concentrations.

Figures 11–13 are generated using three concentrations equal to 0.1, 0.2 and 0.3, respectively. For each concentration, we start with a random distribution for the first calculation of homogenized conductivity. Then, we let the random distribution evolve according either to the DLA or the DMA. The DLA tends to build as quickly as possible a network that looks like a fractal. During the simulation, and especially for high concentration, the fractal characterization seems to not be affected by the increase of the network. The topology of the network increases the conductivity by constructing preferential directions for heat conduction. Now, when the structure evolves according to the DMA, the observations are similar to what can be found in [31]. In fact, a homogeneous nanofluid is described as the dispersion of a discontinuous phase in a continuous one. However, the phase distribution can present three distinct geometric morphologies depending on the volume fraction and shape of the dispersed nanoparticles. These arrangements strongly modify the effective thermo-physical properties at the macro scale. The three geometrical morphologies can be defined as dispersed structure,

aggregated structure, and percolated structure. The percolation threshold is defined as the minimum volume fraction that characterizes the formation of a continuous solid path.

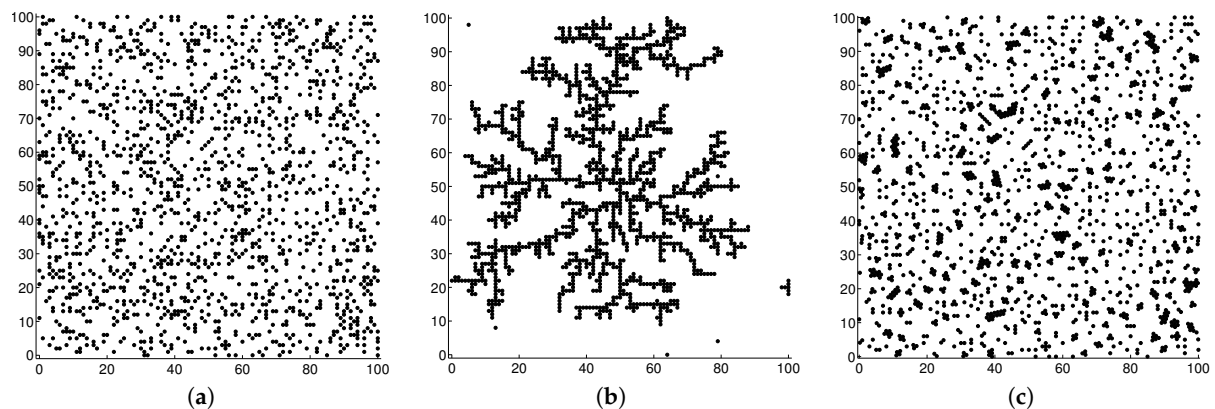


**Figure 11.** Initial random distribution and the resulting enhanced-DLA and MDA-based microstructures for  $C = 0.1$ . (a) Initial; (b) enhanced-DLAa; (c) MDAa.

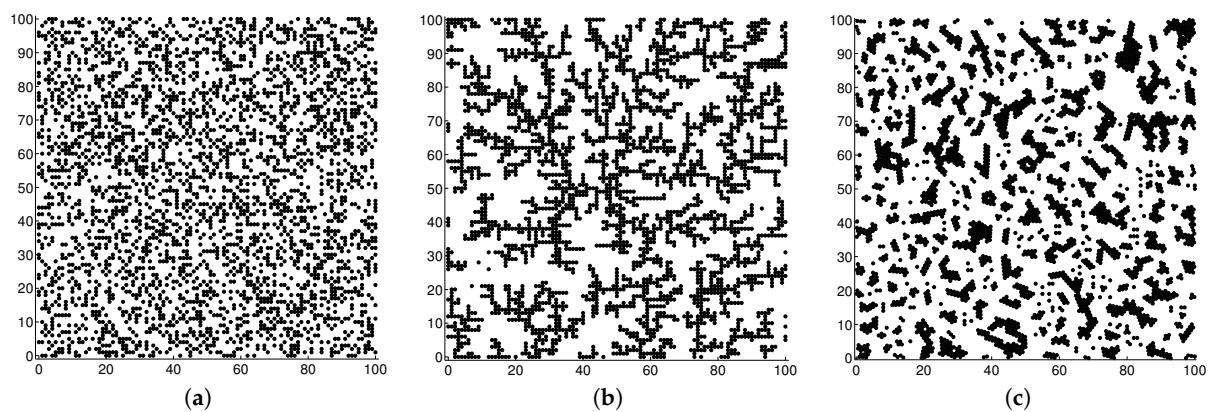


**Figure 12.** Initial random distribution and the resulting enhanced-DLA and MDA-based microstructures for  $C = 0.2$ . (a) Initial; (b) enhanced-DLAa; (c) MDAa.

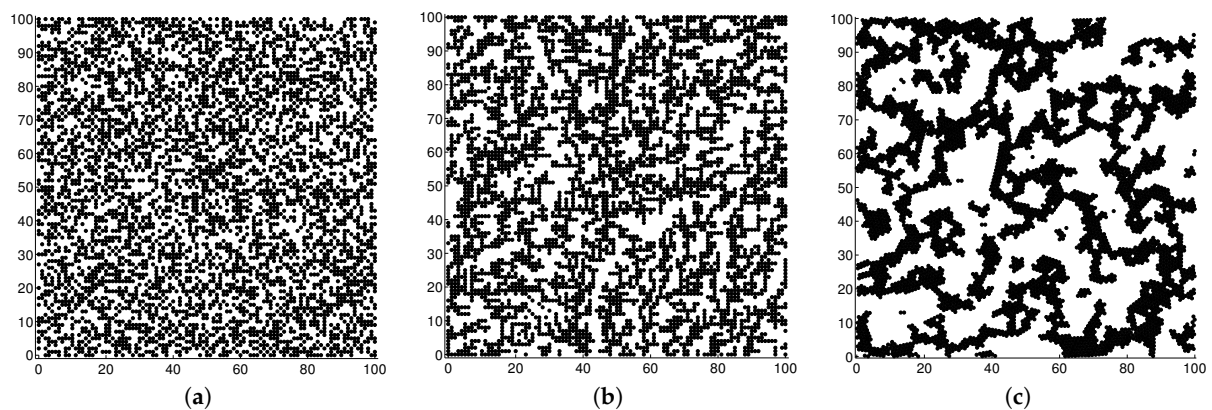


**Figure 13.** Initial random distribution and the resulting enhanced-DLA and MDA-based microstructures for  $C = 0.3$ . (a) Initial; (b) enhanced-DLAa; (c) MDAa.

At low particle concentrations (less than 1%), it can be seen from our calculations (see Figure 9) that the organization of particles (in the form of clusters or fractals) has no noticeable effect on

the thermal conductivity. The results are even comparable to those obtained with the effective medium theory—EMT—(random distribution of individual nanoparticles). Therefore, any unusual enhancement of the thermal conductivity at a low particle fraction must be explained by other arguments than structuration of the nanoparticles in the form of fractals or clusters. The results are quite different at higher particle fractions. It can be seen from our calculations (see Figure 10), for concentrations comprised of between 5% and 20%, that the structuration in the form of fractals (DLA) leads to thermal conductivity enhancements well above what is predicted by the EMT. Unfortunately, the formation of a fractal skeleton within the fluid may have a tragic influence on the rheological properties of the nanofluid, which could even make it unusable from a mechanical point of view. On the other hand, what seems very interesting to us is the positive influence of cluster formation on the thermal conductivity enhancement at fractions higher than 25%, well above EMT and even fractal structuration. This is a very promising result in terms of nanofluid industrial applications because, in our opinion, the cluster's formation has a less damaging influence on the rheological properties of the nanofluid than the fractal skeletons (the validation of this constitutes a work in progress).

## 6. Conclusions

This paper analyzed thermal properties of microstructured fluids and solids, in which the initially dispersed conductive particles aggregate in order to create conductive percolated networks. Two microstructural constructors are analyzed, an enhanced DLAA and the MDAA, from the point of view of the morphology and the associated thermal properties. It has been proved that conductivity is significantly enhanced by the particles structured with respect to a perfectly random particle distribution.

**Acknowledgments:** Francisco Chinesta acknowledges the financial support of the ESI GROUP through its chair at the Ecole Centrale de Nantes.

**Author Contributions:** Amine Ammar was in charge of the proposal and implementation of the different microstructure constructors, Francisco Chinesta proposed the homogenization framework and Rodolphe Heyd defined the general physical framework. All authors have read and approved the final manuscript.

**Conflicts of Interest:** The authors declare no conflict of interest.

## References

1. Pop, E.; Varshney, V.; Roy, A.K. Thermal properties of graphene: Fundamentals and applications. *MRS Bull.* **2012**, *37*, 1273.
2. Choi, U. *Enhancing Thermal Conductivity of Fluids with Nanoparticles*; Technical Report FED; ASME: New York, NY, USA, 1995; Volume 231.
3. Xuan, Y.; Li, Q. Heat transfer enhancement of nanofluids. *Int. J. Heat Transf. Fluid Flow* **2000**, *21*, 58–64.
4. Milanese, M.; Lacobazzi, F.; Colangelo, G.; de Risi, A. An investigation of layering phenomenon at the liquid–solid interface in Cu and CuO based nanofluids. *Int. J. Heat Mass Transf.* **2016**, *103*, 564–571.
5. Mintsu, H.A.; Roy, G.; Nguyen, C.T.; Doucet, D. New temperature dependent thermal conductivity data for water-based nanofluids. *Int. J. Therm. Sci.* **2009**, *48*, 363–371.
6. Gu, B.; Hou, B.; Lu, Z.; Wang, Z.; Chen, S. Thermal conductivity of nanofluids containing high aspect ratio fillers. *Int. J. Heat Mass Transf.* **2013**, *64*, 108–114.
7. Lacobazzi, F.; Milanese, M.; Colangelo, G.; Lomascolo, M.; de Risi, A. An explanation of the Al<sub>2</sub>O<sub>3</sub> nanofluid thermal conductivity based on the phonon theory of liquid. *Energy* **2016**, *116*, 786–794.
8. Sundar, L.S.; Farooq, M.H.; Sarada, S.N.; Singh, M.K. Experimental thermal conductivity of ethylene glycol and water mixture based low volume concentration of Al<sub>2</sub>O<sub>3</sub> and CuO nanofluids. *Int. Commun. Heat Mass Transf.* **2013**, *41*, 41–46.
9. Colangelo, G.; Favale, E.; Miglietta, P.; Milanese, M.; de Risi, A. Thermal Conductivity, Viscosity and Stability of Al<sub>2</sub>O<sub>3</sub>-Diathermic Oil Nanofluids for Solar Energy Systems. *Energy* **2016**, *95*, 124–136.
10. Nnanna, A.G.A. Experimental model of temperature-driven nanofluids. *J. Heat Transf.* **2007**, *129*, 697–704.
11. De Risi, A.; Milanese, M.; Colangelo, G.; Laforgia, D. High efficiency nanofluid cooling system for wind turbines. *Therm. Sci.* **2014**, *18*, 543–554.

12. Yousefi, T.; Veysi, F.; Shojaeizadeh, E.; Zinadini, S. An experimental investigation on the effect of Al<sub>2</sub>O<sub>3</sub>-H<sub>2</sub>O nanofluid on the efficiency of flat-plate solar collectors. *Renew. Energy* **2012**, *39*, 293–298.
13. Lomascolo, M.; Colangelo, G.; Milanese, M.; de Risi, A. Review of heat transfer in nanofluids: Conductive, convective and radiative experimental results. *Renew. Sustain. Energy Rev.* **2015**, *43*, 1182–1198.
14. Philip, J.; Shima, P. Thermal properties of nanofluids. *Adv. Colloid Interface Sci.* **2012**, *183–184*, 30–45.
15. Philip, J.; Shima, P.D.; Raj, B. Nanofluid with tunable thermal properties. *Appl. Phys. Lett.* **2008**, *92*, doi:10.1063/1.2838304.
16. Jain, S.; Patel, H.E.; Das, S.K. Brownian dynamic simulation for the predictions of effective thermal conductivity of nanofluids. *J. Nanopart. Res.* **2009**, *11*, 767–773.
17. Jia, T.; Zhang, Y.; Ma, H.B.; Chen, J.K. Investigation of the characteristics of heat current in a nanofluid based on molecular dynamics simulation. *Appl. Phys. A* **2012**, *108*, 537–544.
18. Estelle, P.; Halefadi, S.; Mare, T. Thermal conductivity of CNT water based nanofluids: Experimental trends and models overview. *J. Therm. Eng.* **2015**, *1*, 381–390.
19. Murshed, S.M.S.; Nieto de Castro, C.A. Superior thermal features of carbon nanotubes-based nanofluids—A review. *Renew. Sustain. Energy Rev.* **2014**, *37*, 155–167.
20. Ma, A.; Chinesta, F.; Ammar, A.; Mackley, M. Rheological modelling of carbon nanotube aggregate suspensions. *J. Rheol.* **2008**, *52*, 1311–1330.
21. Ma, A.; Chinesta, F.; Mackley, M. The rheology and modelling of chemically treated carbon nanotube suspensions. *J. Rheol.* **2009**, *53*, 547–573.
22. Perez, M.; Abisset-Chavanne, E.; Barasinski, A.; Chinesta, F.; Ammar, A.; Keunings, R. On the multi-scale description of electrical conducting suspensions involving perfectly dispersed rods. *Adv. Model. Simul. Eng. Sci.* **2015**, *2*, 23, doi:10.1186/s40323-015-0044-6.
23. Ammar, A.; Mokdad, B.; Chinesta, F.; Keunings, R. A new family of solvers for some classes of multidimensional partial differential equations encountered in kinetic theory modeling of complex fluids. *J. Non-Newton. Fluid Mech.* **2006**, *139*, 153–176.
24. Chinesta, F.; Ammar, A.; Leygue, A.; Keunings, R. An overview of the proper generalized decomposition with applications in computational rheology. *J. Non Newton. Fluid Mech.* **2011**, *166*, 578–592.
25. Doi, M.; Edwards, S.F. Dynamics of rod-like macromolecules in concentrated solution. Part 1. *J. Chem. Soc. Faraday Trans.* **1978**, *2*, 560–570.
26. Ranganathan, S.; Advani, S.G. Fiber-fiber interactions in homogeneous flows of nondilute suspensions. *J. Rheol.* **1991**, *35*, 1499–1522.
27. Toll, S. Note: On the tube model for fiber suspensions. *J. Rheol.* **1993**, *37*, 123–125.
28. Toll, S. Packing mechanics of fiber reinforcements. *Polym. Eng. Sci.* **1998**, *38*, 1337–1350.
29. Chinesta, F.; Ammar, A.; Lemarchand, F.; Beauchene, P.; Boust, F. Alleviating mesh constraints: Model reduction, parallel time integration and high resolution homogenization. *Comput. Methods Appl. Mech. Eng.* **2008**, *197*, 400–413.
30. Lamari, H.; Ammar, A.; Cartraud, P.; Legrain, G.; Jacquemin, F.; Chinesta, F. Routes for efficient computational homogenization of non-linear materials using the proper generalized decomposition. *Arch. Comput. Methods Eng.* **2010**, *17*, 373–391.
31. Lamas, B.; Abreu, B.; Fonseca, A.; Martins, N.; Oliveira, M. Critical analysis of the thermal conductivity models for CNT based nanofluids. *Int. J. Therm. Sci.* **2014**, *78*, 65–76.

